



A shift in the diurnal timing and intensity of deep convection over the Congo Basin during the past 40 years

Kathrin Alber^{a,*}, Liming Zhou^a, Ajay Raghavendra^{a,b}

^a Department of Atmospheric and Environmental Sciences, University at Albany, State University of New York, Albany, NY 12222, USA

^b U.S. Army, Latham, NY 12110, USA

ARTICLE INFO

Keywords:

Congo rainforest
Diurnal cycle
Rainfall
Tropical convection

ABSTRACT

The Congo Basin, one of the three most convective regions in the world, has recently experienced a large-scale drying trend accompanied by an increase in thunderstorm activity. This study analyzes changes in the diurnal variations of cloudiness and deep convection from 1979 to 2019 over the Congo, evaluates their associations with trends in precipitation efficiency, and explores their possible connections to the observed decrease in precipitation. Analyses of GridSat-B1 and MODIS satellite datasets in conjunction with ERA5 reanalysis data show that cloud cover has decreased, and brightness temperature (T_b) has increased during the morning hours, while convective activity has increased and T_b has decreased during the afternoon hours, possibly due to the observed warming and drying trend over the Congo. The combined effects of decreasing clouds during the morning and the subsequent increasing convection during the afternoon have led to an amplification of the diurnal amplitude in T_b over the Congo. Our results also indicate a decrease in precipitation efficiency and an increase in cloud base height. Such changes may be attributable to the Congo drought as increased surface temperatures and decreased surface relative humidity would raise the lifted condensation level, and thus increase the cloud base height and decrease the precipitation efficiency. This positive-feedback mechanism may ultimately result in the observed decrease of precipitation at the surface, further accelerating the drying trend over the Congo.

1. Introduction

The diurnal cycle is one of the most fundamental modes of atmospheric variability attributable to large variations in the solar forcing over the course of the day (Yang and Slingo, 2001). For the rainfall in the tropics, the maximum is reached during the mid- to late afternoon over land and at nighttime over oceans. The maximum rainfall in the afternoon over land is a result of surface solar heating during the day, destabilizing the atmosphere and subsequently encouraging the onset of convection (Yang and Smith, 2006). Over most tropical land areas, mornings are relatively clear, followed by a rapid afternoon buildup of convective clouds associated with a maximum in rainfall and a more gradual decay of clouds during the night (Garreaud and Wallace, 1997). Using water vapor absorption band radiance data from geostationary satellites, Soden (2000) found significant diurnal variations in the upper tropospheric relative humidity in the tropics over both land and oceans, where the variations over land are out of phase with those over the oceans. Tian et al. (2004) showed large diurnal variations in deep

convection, precipitation, and high clouds over deep convective regions. They indicated that upper tropospheric relative humidity peaks around midnight over the oceans and at 03:00 local solar time (LST) over land, with stronger diurnal variations of deep convection over land, which maximizes in the late afternoon and early evening hours.

Central Africa is a hotspot for thunderstorms and one of the most convective regions in the world, characterized by intense thunderstorm activity (Zipser et al., 2006). The Congo Basin, situated in Equatorial Central Africa, is home to the Congo rainforest, the second largest rainforest in the world. Naturally, thunderstorm activity over the Congo is largely influenced by the diurnal cycle, with a morning minimum and a peak in convection and convective rainfall in the late afternoon between 16:00 and 19:00 LST (Yang and Slingo, 2001; Jackson et al., 2009). As most precipitation over the tropics stems from convection (Dai, 2006), the majority of the Congo rainfall originates from deep convection and mesoscale convective systems (MCSs) (Jackson et al., 2009). However, although the Congo experiences some of the most intense thunderstorms and a higher lightning flash rate compared to

* Corresponding author.

E-mail address: kalber2@albany.edu (K. Alber).

<https://doi.org/10.1016/j.atmosres.2021.105869>

Received 24 June 2021; Received in revised form 1 September 2021; Accepted 22 September 2021

Available online 25 September 2021

0169-8095/© 2021 Elsevier B.V. All rights reserved.

other tropical regions (Washington et al., 2013), it receives less precipitation than other equatorial regions like Amazonia or the Indonesian maritime continent. Additionally, surface temperatures in Africa have been rising and are projected to further increase (James and Washington, 2013; Engelbrecht et al., 2015). Furthermore, studies found that the Congo has experienced a large-scale and long-term drying trend, associated with an increase in dry season length (Jiang et al., 2019) and a decrease in mean precipitation since the 1980s (Zhou et al., 2014; Hua et al., 2016, 2018). Counterintuitively, the number, intensity and size of thunderstorms over the Congo have increased (Raghavendra et al., 2018; Alber et al., 2021) despite the decreasing rainfall trend. Hamada et al. (2015) explained this relationship by showing a weak linkage between heavy rainfall and tall thunderstorms, arguing that the tallest thunderstorms do not necessarily produce the most intense rainfall events.

As large parts of the tropical cloudiness and rainfall can be explained by the diurnal cycle (Yang and Slingo, 2001), which is mainly controlled by surface heating, one important question is whether the long-term drought may have modified the diurnal cycle of clouds and deep convection over the Congo. Identifying the diurnal changes in clouds and deep convection over the region promises to enhance our understanding of rainfall patterns and variability as well as associated thunderstorm activity, and may thereby help to reconcile the observed inverse trends in deep convection and rainfall. The goals of this study therefore are to analyze the diurnal cycle of deep convection over the Congo, to investigate its changes from 1979 to 2019, and to ultimately link the changes found in the diurnal cycle of deep convection to the observed decrease in precipitation. The data used is presented in Section 2 and the methods are described in Section 3. In Section 4 we present our results followed by a summary in Section 5.

2. Data

The study domain is the Congo Basin, defined as the area from 5°N to 5°S and 12°E to 30°E. Four datasets were used in this study, 1) the Gridded Satellite (GridSat-B1) (Knapp, 2008; Knapp et al., 2011), 2) MODerate Resolution Imaging Spectroradiometer (MODIS) (Wan et al., 2015a; Wan et al., 2015b), 3) ERA5 reanalysis (Hersbach et al., 2020), and 4) NOAA Climate Prediction Center Precipitation data (CPC) (Sun et al., 2018). All seasons, i.e., December, January, February (DJF), March, April, May (MAM), June, July, August (JJA), and September, October, November (SON) were investigated. MAM and SON are the two wet seasons while DJF and JJA are the two dry seasons receiving lower amounts of precipitation (Pokam et al., 2012; Dyer et al., 2017) as a result of the seasonal shift of the tropical rain belt (Nicholson, 2018). All times of day are indicated in West Africa Standard Time (GMT +1).

2.1. GridSat-B1 satellite data

Climate Data Record quality (NRC, 2004) infrared (IR) channel (11 μm) T_b data sampled by the European Meteorological (MET) series of geostationary satellites from the International Satellite Cloud Climatology Project (ISCCP; Schiffer and Rossow, 1983) was used in this study. The GridSat-B1 T_b data is available at a $0.07^\circ \times 0.07^\circ$ spatial and 3-hourly temporal resolution (Knapp, 2008; Knapp et al., 2011). While the maximum time span available from the GridSat-B1 dataset is from 1981 to present, only the years from 1985 to 2019 were utilized here because of high frequencies of missing data between 1982 and 1985 (Raghavendra et al., 2020). As the atmosphere is almost transparent at 11 μm , the satellite measured radiance was used to derive T_b for cloud top (cloudy-sky) or surface (clear-sky) temperatures.

2.2. MODIS land surface temperature satellite data

MODIS land surface temperature from both Aqua (Wan et al., 2015a) and Terra (Wan et al., 2015b) satellites was further incorporated in this

study. The Aqua and Terra satellites are equipped with the MODIS instruments and image the Earth's surface in 36 spectral bands between 0.405 and 14.385 μm at three spatial resolutions (250 m, 500 m, 1000 m). Terra passes the equator at 10:30 and 22:30 LST, and Aqua passes the equator at 01:30 and 13:30 LST. The MODIS land surface temperature from 2003 to 2019 was obtained from NASA's Land Processes Distributed Active Archive Center (LP DAAC) (e4ftl01.cr.usgs.gov). The MODIS tiles h19v08, h19v09, h20v08 and h20v09, covering the spatial area 10°N to 10°S and 10°E to 30°E, were remapped to 5°N to 5°S and 12°E to 30°E to match the study region. Since daily data often contains missing values, the 8-day composites at 1 km resolution from collection 6 were used (Aqua: MYD11A2; Terra: MOD11A2), providing the best quality clear-sky (cloud-free) land surface temperature measurements from each 8-day period.

2.3. ERA5 reanalysis data

The ERA5 dataset (Hersbach et al., 2020) was used to obtain several variables for the time span from 1979 to 2019 at a $0.25^\circ \times 0.25^\circ$ spatial resolution, i.e., 2-m temperature (T2m), 2-m dew point (D2m), precipitation, cloud base height, and total column water. Additionally, specific humidity and temperature at 4 different pressure levels (i.e., 950 hPa, 850 hPa, 700 hPa and 500 hPa) were used. The time period 1979–2019 was chosen to maximize the temporal coverage. Although the same time period as used for the GridSat-B1 (1985–2019) could have been chosen instead, the results do not change significantly if using the shorter time period. All variables besides precipitation and total column water were obtained at a 3-hourly temporal resolution to match the satellite acquisition times of the GridSat-B1 T_b to ensure the consistency between observed and reanalysis data in terms of temporal resolution. Precipitation and total column water were utilized at a 1-hourly resolution to calculate precipitation efficiency. The ERA5 total column water is defined as the total amount of water including vapor, cloud water and cloud ice, integrated vertically from the ground to the nominal top of the atmosphere. Further, the ERA5 cloud base height, the height above surface of the base of the lowest layer of clouds, is defined as the height of the lowest level with a cloud fraction greater than 1% and a condensate content greater than $1 \times 10^{-6} \text{ kg kg}^{-1}$, where the lowest model layer is not utilized to exclude fog. The temperature and specific humidity at the four pressure levels were utilized to calculate the Gálvez-Davison Index (see Section 3.2), and the T2m and D2m served to retrieve the 2-m relative humidity (RH2m) using the improved Magnus formula (Alduchov and Eskridge, 1996). The ERA5 precipitation is provided by the Global Precipitation Climatology Project (GPCP) based on satellite data and the Global Precipitation Climatology Centre (GPCC) which also includes rain-gauge observations. Although other reanalysis products could have been utilized for this analysis, it is difficult to identify the most accurate dataset over the Congo Basin due to the extremely limited surface observations such as gauge stations and radiosonde networks. However, Hua et al. (2019) showed that the bias and root-mean-square error associated with the ERA-Interim reanalysis dataset is comparable to other reanalysis products, and Gleixner et al. (2020) found that the ERA5 matched the observations over Africa even better than the ERA-Interim data. Therefore, the ERA5 dataset was decided to be appropriate for this study.

2.4. CPC precipitation data

To compare ERA5 hourly reanalysis precipitation to daily gauge-based products, the NOAA Climate Prediction Center (CPC) global unified gauge-based daily precipitation was further used, where gauge observations were merged with satellite derived data (Sun et al., 2018). The dataset was provided by the NOAA/OAR/ESRL PSL and was obtained online (psl.noaa.gov/) at a $0.5^\circ \times 0.5^\circ$ spatial resolution.

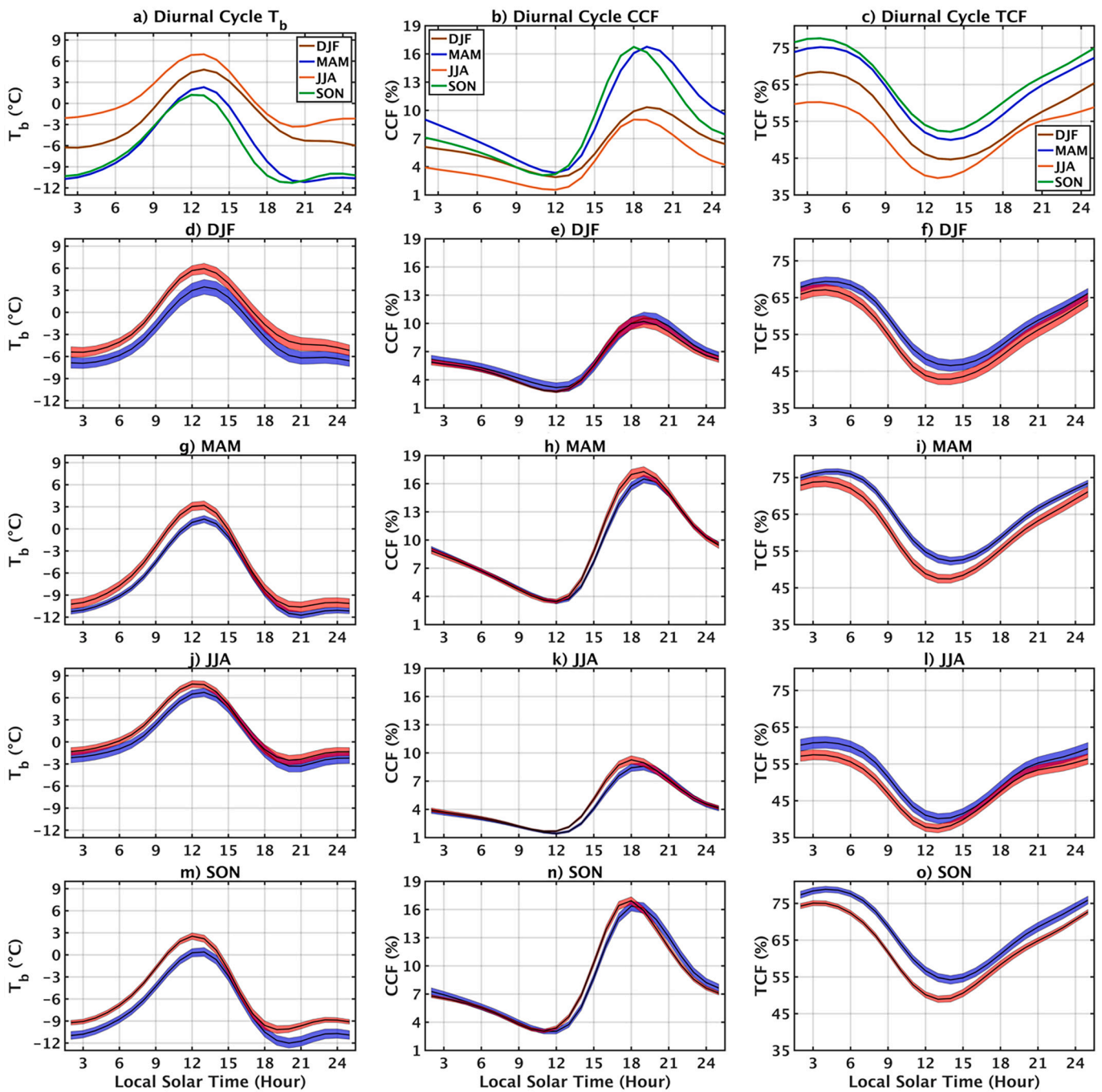


Fig. 1. Diurnal cycles of (a), (d), (g), (j), (m) GridSat-B1 T_b ($^{\circ}\text{C}$), (b), (e), (h), (k), (n) GridSat-B1 CCF (%), and (c), (f), (i), (l), (o) GridSat-B1 TCF (%). Averaged over the study domain. (a), (b) and (c): Seasonal averages over the years 1985–2019. (d)–(o): Averages over the years 1985–1996 and 2008–2019 (black lines) with the respective 95% confidence intervals shown separately, where the blue color represents the years 1985–1996 and the red color represents the years 2008–2019. (For interpretation of the references to color in this figure legend, the reader is referred to the web version of this article.)

3. Methods

3.1. Thunderstorm and cloud detection

To detect thunderstorm activity, the GridSat-B1 data was used and the fraction of pixels with T_b lower than -50°C (e.g., Alber et al., 2021) within each $0.07^{\circ} \times 0.07^{\circ}$ grid over the study domain was estimated from the GridSat-B1 data. The fraction of pixels with T_b lower than -50°C was defined as cold cloud fraction (CCF). Since deep tropical convection is characterized by lower values of T_b , the CCF was used to represent areas in which deep convection occurs (Taylor et al., 2017;

Hart et al., 2019). To detect the total cloud fraction (TCF), the fraction of pixels with T_b lower than $+10^{\circ}\text{C}$ within each $0.07^{\circ} \times 0.07^{\circ}$ grid was further calculated. The TCF was used to estimate the amount of all cloud types, including mid- to low-level clouds. Although the threshold $+10^{\circ}\text{C}$ was used for this study, other thresholds (i.e., 0°C , $+5^{\circ}\text{C}$, $+15^{\circ}\text{C}$) have been tested as well and showed similar results.

3.2. Gálvez-Davison Index

To measure the thunderstorm potential over the region, the Gálvez-Davison Index (GDI) was used (e.g., Alber et al., 2021). The GDI is a

thermodynamic index, developed by Michael Davison and José Gálvez at NOAA's Weather Prediction Center (WPC). This index can forecast convection in the tropics more accurately than traditional indices by focussing on thermodynamic processes rather than dynamical processes. The GDI, a unitless parameter, is used diagnostically, where higher values indicate a higher potential for thunderstorms. To calculate the GDI, temperature and specific humidity values are needed at four different levels, i.e., at 950 hPa, 850 hPa, 700 hPa, and 500 hPa (Gálvez and Davison, 2016). In this study, ERA5 temperature and specific humidity data at these levels were used at a 3-hourly resolution for the GDI calculation. A complete derivation and explanation of the GDI is presented in Gálvez and Davison (2016) and Alber et al. (2021).

3.3. Precipitation efficiency

Precipitation efficiency was used to evaluate how efficiently the convective systems produce precipitation by measuring how much of the water condensing in a rising column of air eventually reaches the surface as precipitation (Lau and Wu, 2003; Sui et al., 2007; Lutsko and Cronin, 2018). While there are numerous techniques to calculate precipitation efficiency, in this study the ratio between rainfall and total column water was used to estimate the precipitation efficiency. More specifically, the hourly ERA5 precipitation values were summed up to daily total precipitation, and the daily average ERA5 total column water was calculated from the hourly total column water. To determine the precipitation efficiency, the total daily precipitation was divided by the daily average total column water (Sellers, 1965; Market et al., 2003).

3.4. Diurnal cycle analysis

The seasonally averaged diurnal cycles were calculated for T_{2m}, RH_{2m}, and cloud base height from the ERA5 dataset for the years 1979–2019, and for T_b, CCF and TCF from the GridSat-B1 product for the years 1985–2019. Temporal changes of the diurnal cycles of T_b, CCF, TCF, T_{2m}, RH_{2m}, cloud base height, and GDI were analyzed by comparing the averages and 95% confidence intervals of two groups with different time periods. The first group was calculated by averaging over the first third of the time span analyzed, i.e., 1985–1996, while the second group represented the average of the last third of the time span analyzed, i.e., 2008–2019. This method helped to analyze changes in the diurnal cycle by determining if the 95% confidence interval of first third is significantly different from the 95% confidence interval of the last third, where the 95% confidence intervals were determined by multiplying the standard error with the 95% probability intervals of the t-distribution at each timestep. The diurnal cycles were calculated using a 3–24-hour spectral filter. The discrete Fourier transform (DFT) was applied to the anomaly data using a fast Fourier transform (FFT) in order to extract the diurnal cycles (e.g., Frigo and Johnson, 1998, 2005; Tian et al., 2004). To do so, the 3-hourly data was first interpolated to 1-hourly resolution by applying the spline interpolation method to acquire more datapoints for a more detailed analysis and to prevent spectral aliasing by using a 3-hour filter. This interpolation of the 3-hourly to 1-hourly data may introduce some uncertainties associated with indicating specific hours of the day after interpolating. Additionally, since thunderstorms over the Congo Basin normally propagate from the East African Highlands westwards over the Congo Basin, the time of peak convection (e.g., highest percentage of CCF) is earlier in the eastern parts of the study domain compared to the western areas. As time averages over the whole domain were used for this study, the peak times of CCF deviate slightly from the indicated values depending on the region.

The diurnal T_b amplitude was further obtained by subtracting the values averaged over 12:00–13:00 LST from the values averaged over 18:00–19:00 LST, where 12:00–13:00 LST is the time of maximum T_b or minimum convection, and the values at 18:00–19:00 LST represent the lowest T_b values when the CCF is highest, and convection is deepest. The diurnal T_{2m} amplitude was calculated by subtracting the values

averaged over 04:00–06:00 LST, i.e., the time of minimum T_{2m}, from the values averaged over 13:00–15:00 LST, i.e., the time of maximum T_{2m}. To calculate the diurnal MODIS land surface temperature amplitude, the MODIS data was interpolated to 2-hourly data since the equator passing times of Aqua and Terra are not ideal to calculate the diurnal land surface temperature amplitude and the available times do not match the times used to calculate the T_{2m} ERA5 amplitude. After interpolating the dataset, the values at 05:30 LST and the values averaged over 13:30 and 15:30 LST (i.e., 14:30 LST) were chosen to calculate the diurnal land surface temperature amplitude.

3.5. Trend analysis

The linear trends of the ERA5 and CPC precipitation, ERA5 precipitation efficiency, and the diurnal amplitudes of the GridSat-B1 T_b, MODIS land surface temperature and ERA5 T_{2m} were determined in order to identify changes of the different variables. Linear trends were calculated based on least squares regression and the statistical significance (p-value) of the linear regression was evaluated using the two-tailed Student's t-test.

4. Results

The seasonally averaged diurnal T_b cycles in Fig. 1a show generally higher T_b values during the two dry seasons and lower values during the two wet seasons. The T_b is highest at 12:00 LST during SON (1.2 °C), and at 13:00 LST during DJF (4.8 °C), MAM (2.3 °C), and JJA (7.0 °C), while it is lowest at 20:00 LST during JJA (−3.3 °C) and SON (−11.3 °C), at 21:00 LST during MAM (−11.2 °C), and at 03:00 LST during DJF (−6.3 °C). Fig. 1b is similar to Fig. 1a but for the CCF, with a maximum at 18:00 LST during JJA (9.0%) and SON (16.7%), and at 19:00 LST during DJF (10.3%) and MAM (16.8%). The lowest percentage of CCF is recorded at 11:00 LST during SON (3.1%), and at 12:00 LST during DJF (2.3%), MAM (3.3%) and JJA (1.5%). The CCF is generally higher during the two wet seasons than the two dry seasons. Fig. 1c shows a minimum in TCF at 13:00 LST during JJA (39.6%), and at 14:00 LST during DJF (44.6%), MAM (50.0%) and SON (52.2%), while the maximum is at 04:00 LST during all seasons (68.5% for DJF; 75.2% for MAM; 60.2% for JJA; 77.6% for SON). Overall, the highest T_b values at 12:00–13:00 LST and the lowest TCF values at 13:00–14:00 LST indicate a minimum in cloud cover around noon and in the early afternoon, while the maximum in CCF at 18:00–19:00 LST suggests that convection is deepest around sunset. Consequently, the minimum in the diurnal cycle of deep convection and convective rainfall is recorded right after noon and the maximum around sunset.

To investigate changes in the diurnal cycles of T_b, CCF and TCF, the diurnal cycles averaged over the years 1985–1996 (first third) and 2008–2019 (last third) are shown in Figs. 1d–o, together with the respective 95% confidence intervals. For the T_b (Figs. 1d, g, j and m), values have increased during the last third when compared to the first third during all seasons, especially in the morning and early afternoon hours until around 14:00 LST. More specifically, the 95% confidence intervals indicate significant differences (p < 0.05) between the first and last third from 02:00–15:00 LST and 20:00–21:00 LST during DJF, 02:00–14:00 LST and 22:00–23:00 LST during MAM, 07:00–13:00 LST during JJA, and 01:00–14:00 LST and 19:00–24:00 LST during SON. Consequently, the T_b has increased significantly during all seasons in the mornings, possibly due to a decrease of clouds in the morning and early afternoon, as well as in the late evening. Further, the amount of CCF has increased, mainly in the afternoon hours (Figs. 1e, h, k and n). While the 95% confidence intervals of the first and last third are not different during DJF, they are different from 14:00–18:00 LST during MAM, 12:00–17:00 LST during JJA, and 13:00–17:00 LST during SON, indicating a shift to a higher percentage of CCF in the afternoon during all seasons besides DJF, suggesting that thunderstorm activity in the afternoon has been increasing. This is consistent with previous studies

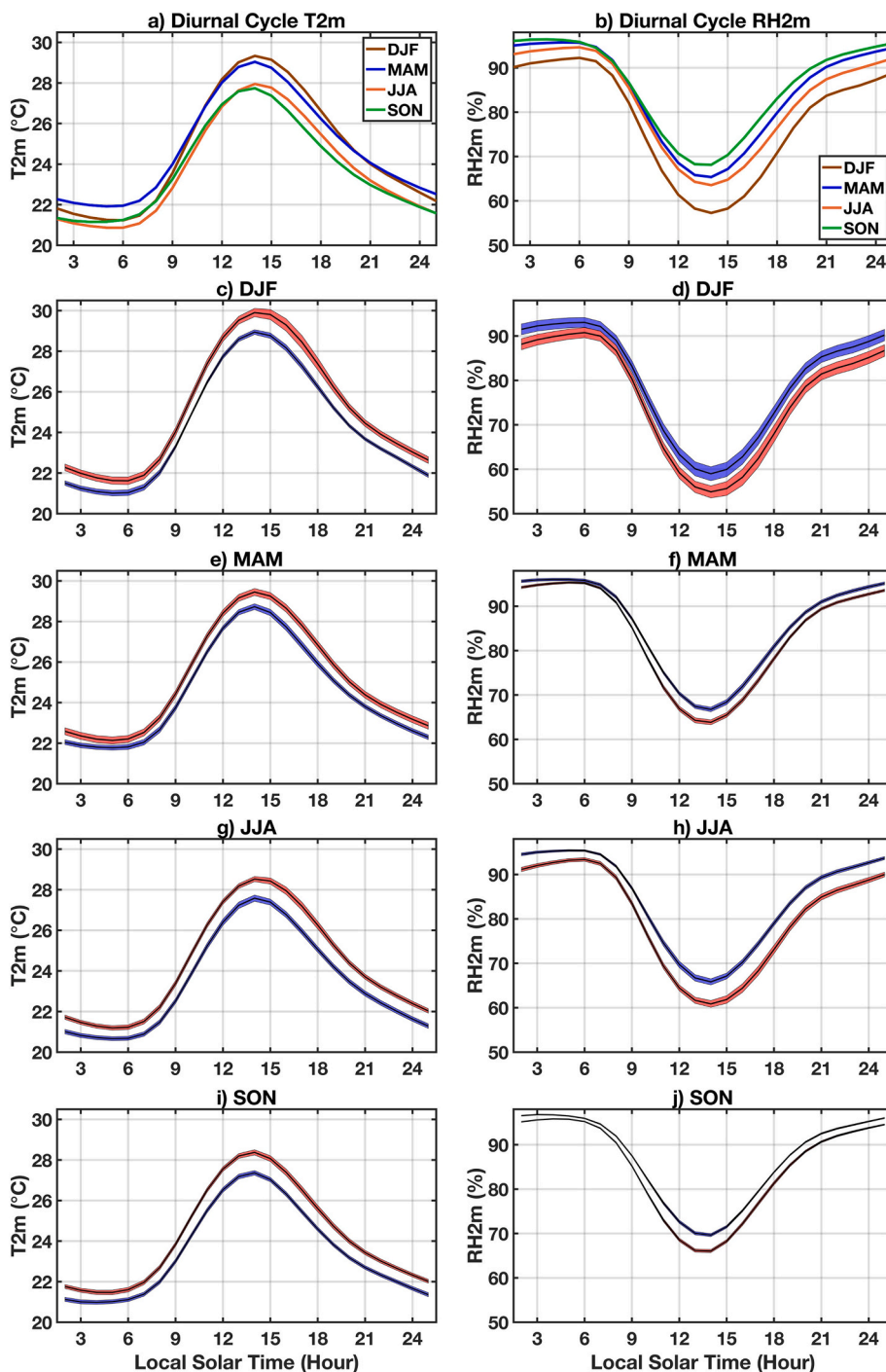


Fig. 2. Diurnal cycles of (a), (c), (e), (g), (i) ERA5 T2m (°C), and (b), (d), (f), (h), (j) ERA5 RH2m (%). Averaged over the study domain. (a) and (b): Seasonal averages over the years 1979–2019. (c)–(j): Averages over the years 1985–1996 and 2008–2019 (black lines) with the respective 95% confidence intervals shown separately, where the blue color represents the years 1985–1996 and the red color represents the years 2008–2019. (For interpretation of the references to color in this figure legend, the reader is referred to the web version of this article.)

showing an intensification of MCSs during the month of February (Taylor et al., 2018), and a general increase in mean convective activity across Africa (Hart et al., 2019). Changes in TCF (Figs. 1f, i, l and o) confirm that the amount of clouds has been decreasing in the morning hours, where the 95% confidence intervals of the first and last third are different from 06:00–15:00 LST during DJF, 03:00–24:00 and 01:00 LST during MAM, 02:00–13:00 LST during JJA, and 01:00–24:00 LST during SON, with lower TCF during the later period. Overall, the increased T_b and decreased TCF in the morning, and the increased CCF during the afternoon suggest a decreasing trend in clouds in the morning and a tendency towards stronger and more intense convection in the afternoon in recent years.

To corroborate the above changes of the diurnal cycles of clouds and

deep convection obtained from satellite data, the same analysis was conducted using ERA5 T2m and RH2m from 1979 to 2019. Figs. 2a and b show the seasonally averaged diurnal cycles of T2m and RH2m, with a T2m maximum at 14:00 LST during all seasons (29.3 °C for DJF; 29.0 °C for MAM; 28.0 °C for JJA; 27.7 °C for SON), and a minimum at 04:00 LST during SON (21.1 °C), 05:00 LST during MAM (21.9 °C), and at 06:00 LST during DJF (21.2 °C) and JJA (20.9 °C). The RH2m maxima are recorded at 04:00 LST during SON (96.4%), 05:00 LST during MAM (95.7%), and at 06:00 LST during DJF (92.2%) and JJA (94.6%), while the RH2m minima are at 14:00 LST during all seasons (57.3% for DJF; 65.4% for MAM; 63.5% for JJA; 68.1% for SON). Furthermore, changes in the diurnal RH2m and T2m cycles (Figs. 2c–j) indicate a general warming and drying trend, where the T2m has increased significantly

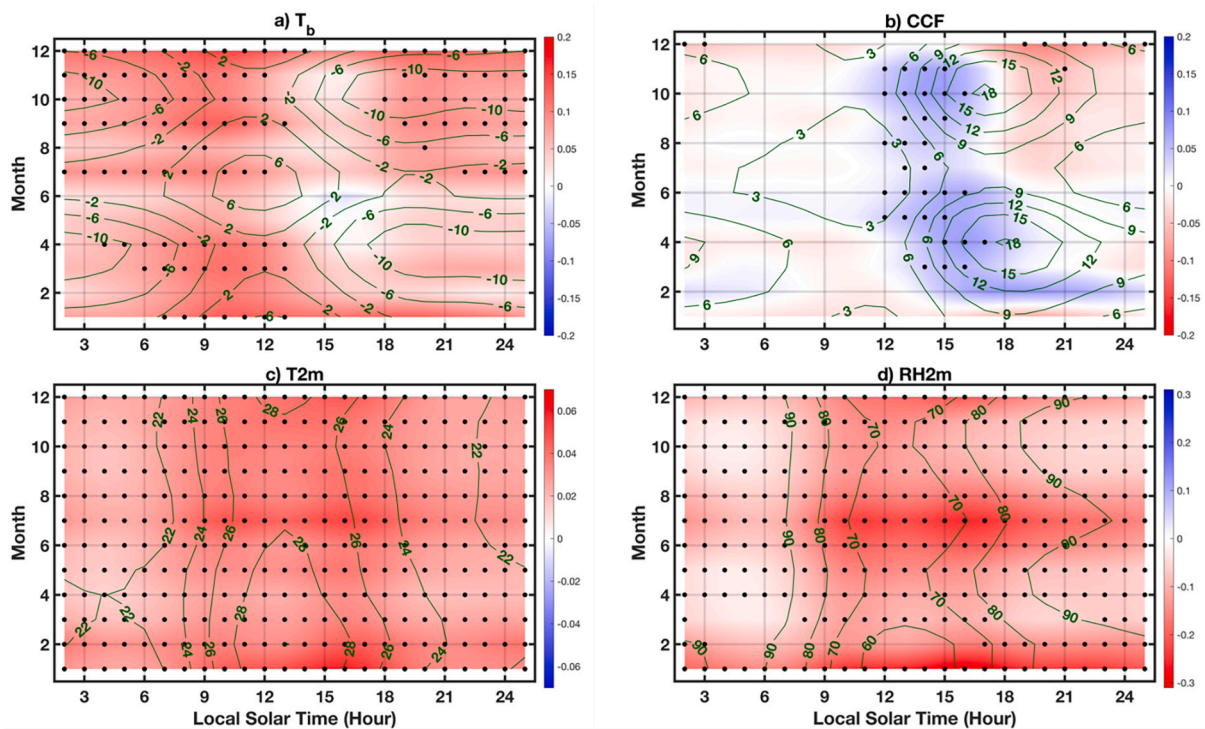


Fig. 3. Trends in (a) GridSat-B1 T_b ($^{\circ}\text{C year}^{-1}$) from 1985 to 2019, (b) CCF ($\% \text{ year}^{-1}$) from 1985 to 2019, (c) ERA5 T_{2m} ($^{\circ}\text{C year}^{-1}$) from 1979 to 2019, and (d) ERA5 RH_{2m} ($\% \text{ year}^{-1}$) from 1979 to 2019. Averaged over the study domain. Trends significant at $p < 0.05$ are shown using a black dot. The green lines show the climatological values of T_b ($^{\circ}\text{C}$) and CCF ($\%$) from 1985 to 2019, and ERA5 T_{2m} ($^{\circ}\text{C}$) and RH_{2m} ($\%$) from 1979 to 2019. (For interpretation of the references to color in this figure legend, the reader is referred to the web version of this article.)

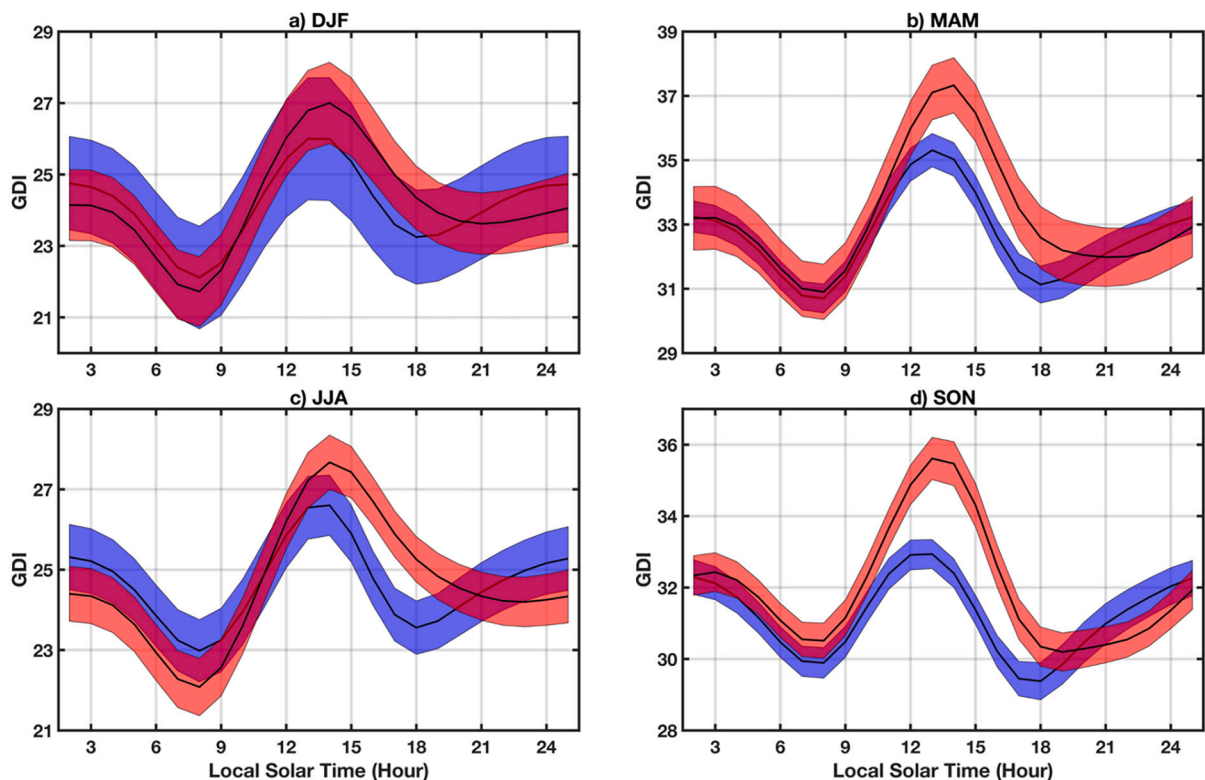


Fig. 4. Diurnal cycles of the GDI averaged over the study domain. Averages over the years 1985–1996 and 2008–2019 (black lines) with the respective 95% confidence intervals shown separately, where the blue color represents the years 1985–1996 and the red color represents the years 2008–2019. (For interpretation of the references to color in this figure legend, the reader is referred to the web version of this article.)

Table 1
Trends in CCF ($10^{-2} \times \% \text{ yr}^{-1}$) for the different seasons and hours in the afternoon from 1985 to 2019.

| | DJF | MAM | JJA | SON |
|--------|-------|-------|-------|-------|
| 13 LST | -1.29 | 1.52 | 1.66* | 3.35* |
| 14 LST | -0.62 | 3.11* | 2.69* | 5.12* |
| 15 LST | 0.01 | 4.90* | 3.67* | 6.39* |
| 16 LST | 0.37 | 6.31* | 4.18* | 6.65* |
| 17 LST | 0.14 | 6.65* | 3.75* | 5.41* |
| 18 LST | -0.80 | 5.51* | 2.15 | 2.47 |
| 19 LST | -2.01 | 3.54 | 0.37 | -1.04 |

Values significant at the 95% level are indicated by an asterisk (*).

during all hours of the day and all seasons. The RH2m increased during all hours and seasons as well, besides at 07:00 LST during DJF where the changes are not significant.

The increase in T_b in the morning hours and in CCF during the afternoon are also illustrated in Figs. 3a and b, while Figs. 3c and d show the general increase of the T2m and the decrease of the RH2m. More specifically, the T_b increased significantly ($p < 0.05$) in the morning during all months besides February, May and June, while trends in the afternoon are insignificant (Fig. 3a). Additionally, trends in CCF (Fig. 3b) show significant increases in the afternoon during all months except January, February and December. This is generally consistent with the results from Fig. 2, confirming that T_b has increased in the morning while convection intensified in the afternoon.

To investigate changes in thunderstorm potential, the diurnal cycles of the GDI averaged over the first (1985–1996) and last (2008–2019) third are shown in Fig. 4, together with the according 95% confidence intervals. While there are no significant changes during DJF, the GDI increased significantly ($p < 0.05$) in the afternoon from 13:00–17:00 LST during MAM, from 15:00–18:00 LST during JJA, and from

11:00–17:00 LST during SON. As the GDI is used as a forecasting tool, this confirms that thunderstorm potential has increased in the afternoon and evening hours, complementing the findings in Figs. 1 and 3.

Table 1 lists the trends of the CCF for the years 1985–2019 and the hours 13:00–19:00 LST. The CCF has increased significantly ($p < 0.05$) from 14:00–17:00 LST during all seasons except DJF. More specifically, the increase in CCF is largest at 16:00 LST during JJA ($4.18 \times 10^{-2} \% \text{ year}^{-1}$) and SON ($6.65 \times 10^{-2} \% \text{ year}^{-1}$), and at 17:00 LST during MAM ($6.65 \times 10^{-2} \% \text{ year}^{-1}$) while DJF does not show any significant trends. Consequently, thunderstorms have intensified the most during the afternoon buildup period, and not during the time of maximum deep convection around sunset. The increased thunderstorm intensity during the buildup period may possibly be a result of the surface warming and drying trend associated with the long-term Congo drought and the subsequent decrease in cloud cover in the morning, leading to increased heating and an earlier onset of convection since the convective temperature is reached earlier. The increase in T2m might eventually lead to a shift in the maximum of CCF to an earlier time of day. Fig. 5 confirms this hypothesis, where the blue boxplots represent the percentage of CCF averaged over the years 1985–1996 (first third) at 13:00–19:00 LST, and the red boxplots show the same for the years 2008–2019 (last third). The results in Fig. 5 are consistent with the trends listed in Table 1. The notches of the boxplots of the first and last third for DJF overlap for all times, indicating that they are not significantly different. During MAM, the CCF increased significantly ($p < 0.05$) from 14:00–18:00 LST. For JJA and SON, the differences between the first and last third are significant ($p < 0.05$) from 13:00–17:00 LST, indicating increased CCF in the afternoon hours during all seasons besides DJF. Additionally, the maximum percentage of CCF generally shifted to earlier in the day during all seasons.

The interannual variability and linear trends of the diurnal T_b amplitude are displayed in Fig. 6. The diurnal T_b amplitude has

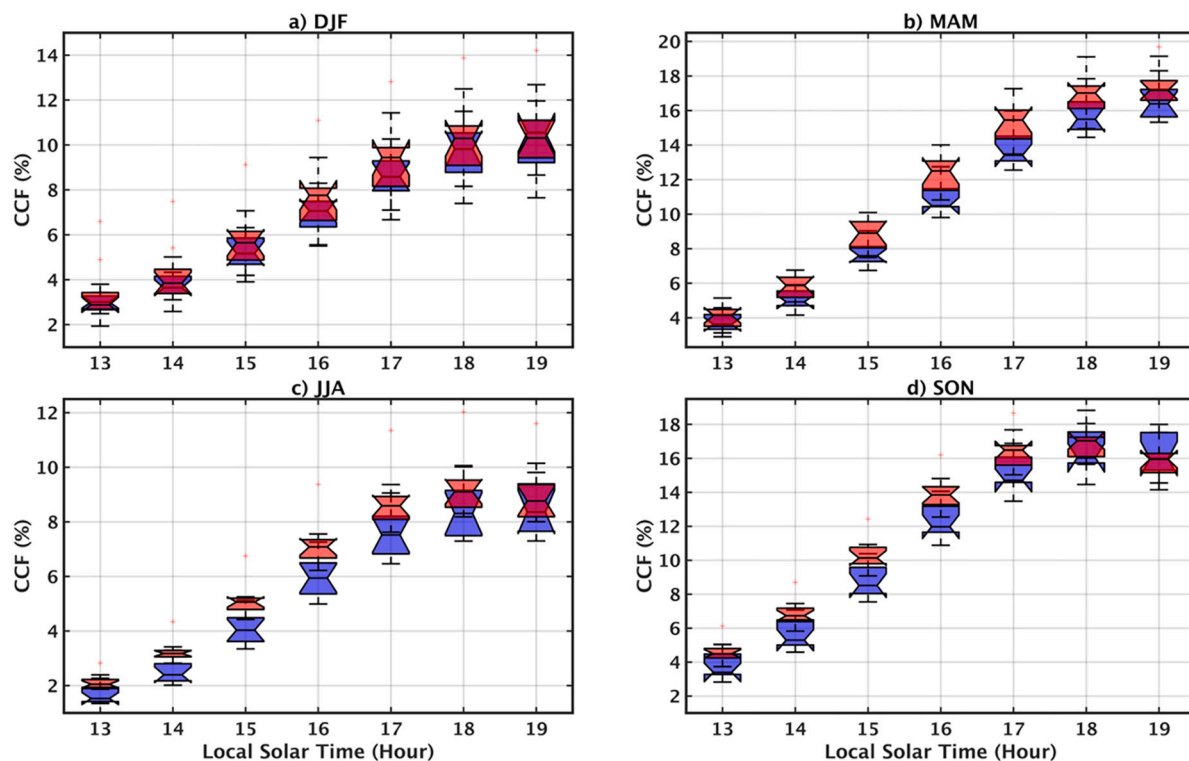


Fig. 5. CCF (%) at the different times of day (LST) averaged over the first third (1985–1996; blue color) and the last third of the time period analyzed (2008–2019; red color) for the different seasons. Averaged over the study domain. The central black bar on each box represents the median, the edges of the box indicate the 25th and the 75th percentiles, and the notches represent the 95% confidence intervals of the median. The upper and lower whiskers show the variability outside the upper and lower quartiles while outliers are plotted as red crosses. (For interpretation of the references to color in this figure legend, the reader is referred to the web version of this article.)

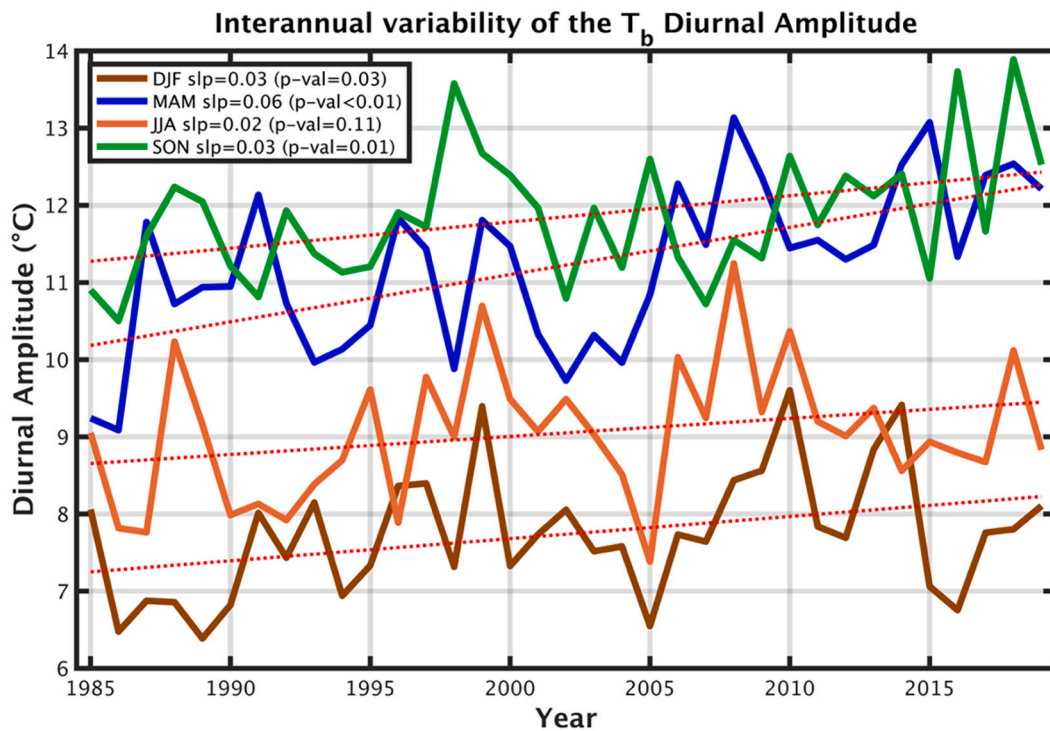


Fig. 6. Interannual variability and linear trends ($^{\circ}\text{C year}^{-1}$) of the diurnal amplitude of GridSat-B1 T_b (12:00–13:00 LST vs. 18:00–19:00 LST) from 1985 to 2019, averaged over the study domain.

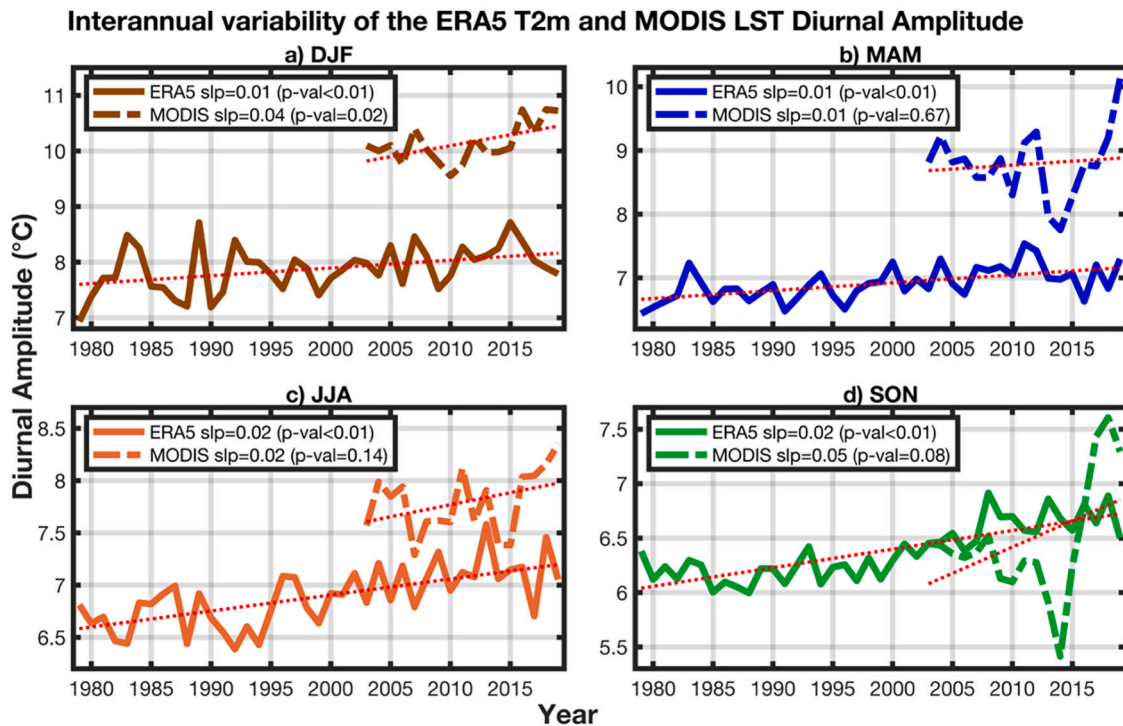


Fig. 7. Solid lines: Interannual variability and linear trends ($^{\circ}\text{C year}^{-1}$) of the diurnal amplitude of ERA5 T2m (04:00–06:00 LST vs. 13:00–15:00 LST) from 1979 to 2019. Dashed lines: Interannual variability and linear trends ($^{\circ}\text{C year}^{-1}$) of the diurnal amplitude of MODIS land surface temperature (05:30 LST vs. 13:30–15:30 LST) from 2003 to 2019. Averaged over the study domain.

increased significantly ($p < 0.05$) during all seasons besides JJA, with the largest increase during MAM ($0.06\text{ }^{\circ}\text{C year}^{-1}$), followed by DJF ($0.03\text{ }^{\circ}\text{C year}^{-1}$) and SON ($0.03\text{ }^{\circ}\text{C year}^{-1}$). Consistent with the trends of the diurnal T_b amplitude, the diurnal T2m amplitude has increased by

$0.01\text{ }^{\circ}\text{C year}^{-1}$ ($p < 0.05$) during DJF and MAM, and $0.02\text{ }^{\circ}\text{C year}^{-1}$ ($p < 0.05$) during JJA and SON (Fig. 7, solid lines). The trends of the ERA5 T2m diurnal amplitude are further compared to the MODIS land surface temperature (Fig. 7, dashed lines). The diurnal land surface temperature

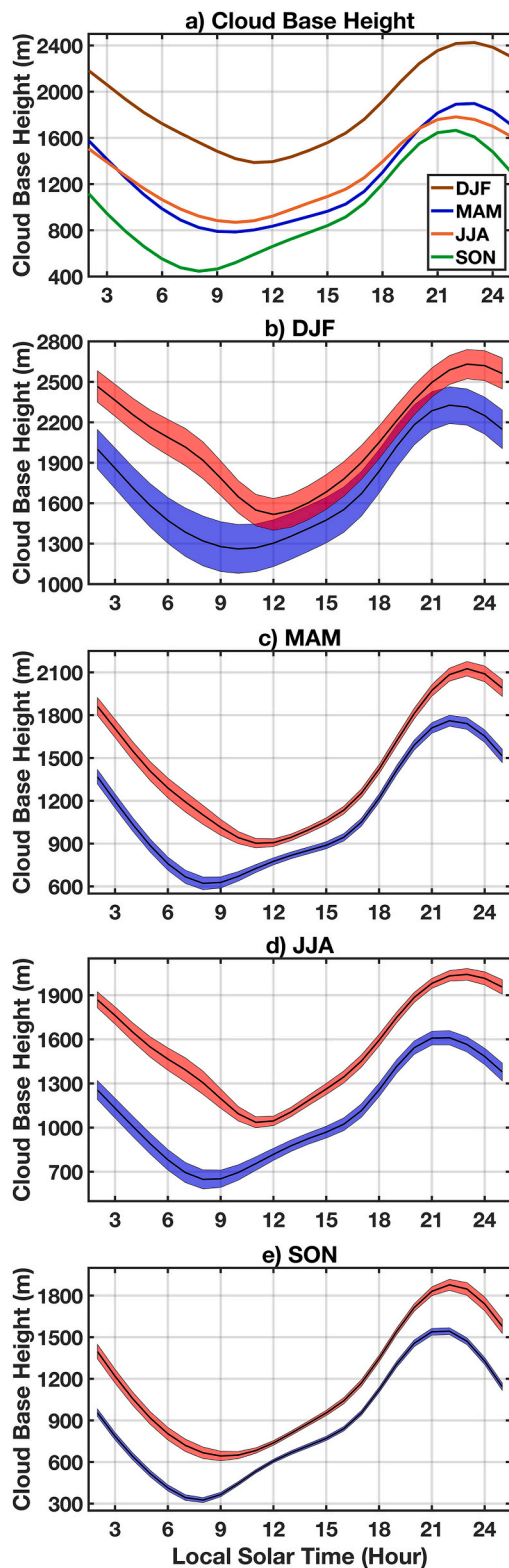


Fig. 8. Diurnal cycles of the ERA5 cloud base height (m) averaged over the study domain. (a): Seasonal averages over the years 1979–2019. (b)–(e): Averages over the years 1985–1996 and 2008–2019 (black lines) with the respective 95% confidence intervals shown separately, where the blue color represents the years 1985–1996 and the red color represents the years 2008–2019. (For interpretation of the references to color in this figure legend, the reader is referred to the web version of this article.)

amplitude shows a significant increasing trend during DJF ($0.04\text{ }^{\circ}\text{C}$; $p < 0.05$) and SON ($0.05\text{ }^{\circ}\text{C}$; $p < 0.10$). The increase found during all seasons in the $T_2\text{m}$ diurnal amplitude, during DJF, MAM and SON in the T_b diurnal amplitude, and during DJF and SON in the land surface temperature diurnal amplitude complement the findings from Figs. 4 and 5, indicating an increase in the diurnal amplitude due to a decrease of clouds in the morning and more vigorous convection in the afternoon, which may be caused by the increased heating and drying observed over the region.

Fig. 8a illustrates the diurnal variations in cloud base height for the different seasons, with a minimum in the morning hours and a maximum in the evening. More specifically, the minimum is recorded at 08:00 LST during SON (445.9 m), 10:00 LST during MAM (785.8 m) and JJA (869.3 m), and at 11:00 LST during DJF (1387.0 m). The maxima are at 23:00 LST during all seasons (2432.7 m for DJF; 1899.6 m for MAM; 1765.1 m for JJA; 1615.1 m for SON). Figs. 8b–e further show a general increase in cloud base height during all hours of the day during MAM, JJA and SON, and from 01–10:00 LST and 22:00–24:00 LST during DJF. The increase is most pronounced during the early morning hours and can be explained by the surface warming and drying trend in the study region, as increasing the $T_2\text{m}$ and decreasing the RH_2m will raise the lifted condensation level and ultimately increase the cloud base height.

Consistent with the observed drought over the Congo, the trends of both the ERA5 and CPC precipitation are decreasing during all seasons (Figs. 9a–d). Further, the trends in precipitation efficiency (Fig. 9e) have decreased significantly during all seasons, with the strongest decrease of $-0.10\% \text{ year}^{-1}$ ($p < 0.05$) during DJF, MAM and SON, followed by a decrease of $-0.08\% \text{ year}^{-1}$ ($p < 0.05$) during JJA. The decreasing precipitation efficiency may be a result of the increased cloud base height, leading to an increase in virga and less precipitation reaching the surface (see more discussion in Section 5).

5. Discussion and conclusions

In this study, changes in the diurnal cycles of clouds, deep convection and other variables including $T_2\text{m}$ and RH_2m were analyzed over the Congo Basin from 1979 to 2019. The aim of this analysis is to explain and link the changes in the diurnal cycle of deep convection, the decrease in precipitation, and the drying trend observed over the region. The diurnal cycles of T_b , CCF, TCF, $T_2\text{m}$, RH_2m , cloud base height and GDI were calculated, and their changes were identified and analyzed using a 3–24-hour spectral filter. Further, the long-term trends of the diurnal T_b , land surface temperature, and $T_2\text{m}$ amplitudes, the CCF, precipitation and precipitation efficiency were investigated.

The results show a maximum in T_b at 12:00–13:00 LST and a minimum in TCF at 13:00–14:00 LST, while a maximum in CCF was found at 18:00–19:00 LST, indicating a minimum in clouds around noon and in the early afternoon, and a peak in deep convection around sunset. Additionally, trends show that the T_b has increased and the TCF has decreased in the morning, suggesting a decrease of cloudiness during the morning hours. In the afternoon, the GDI and CCF have increased where the strongest increase in CCF was detected at around 16:00 LST. This shows increased thunderstorm activity, especially during the afternoon build up period, which is consistent with previous findings showing increased MCS intensity over the Congo (e.g., Raghavendra et al., 2018; Taylor et al., 2018) and enhanced mean convective activity across Africa (Hart et al., 2019). Furthermore, the maximum in CCF shifted to earlier in the day, suggesting that the increased heating and the decrease of clouds in the morning may lead to an earlier onset of convection. Results also show that the diurnal amplitude of convection over the Congo has increased, with the increase in the T_b amplitude reaching from $0.03\text{ }^{\circ}\text{C year}^{-1}$ to $0.06\text{ }^{\circ}\text{C year}^{-1}$, depending on the season. This may be the combined effect of the decrease in clouds found in the morning and an increase of deep convection in the afternoon.

The enhanced convection found in the study region during recent years may be caused by the observed long-term warming and drying

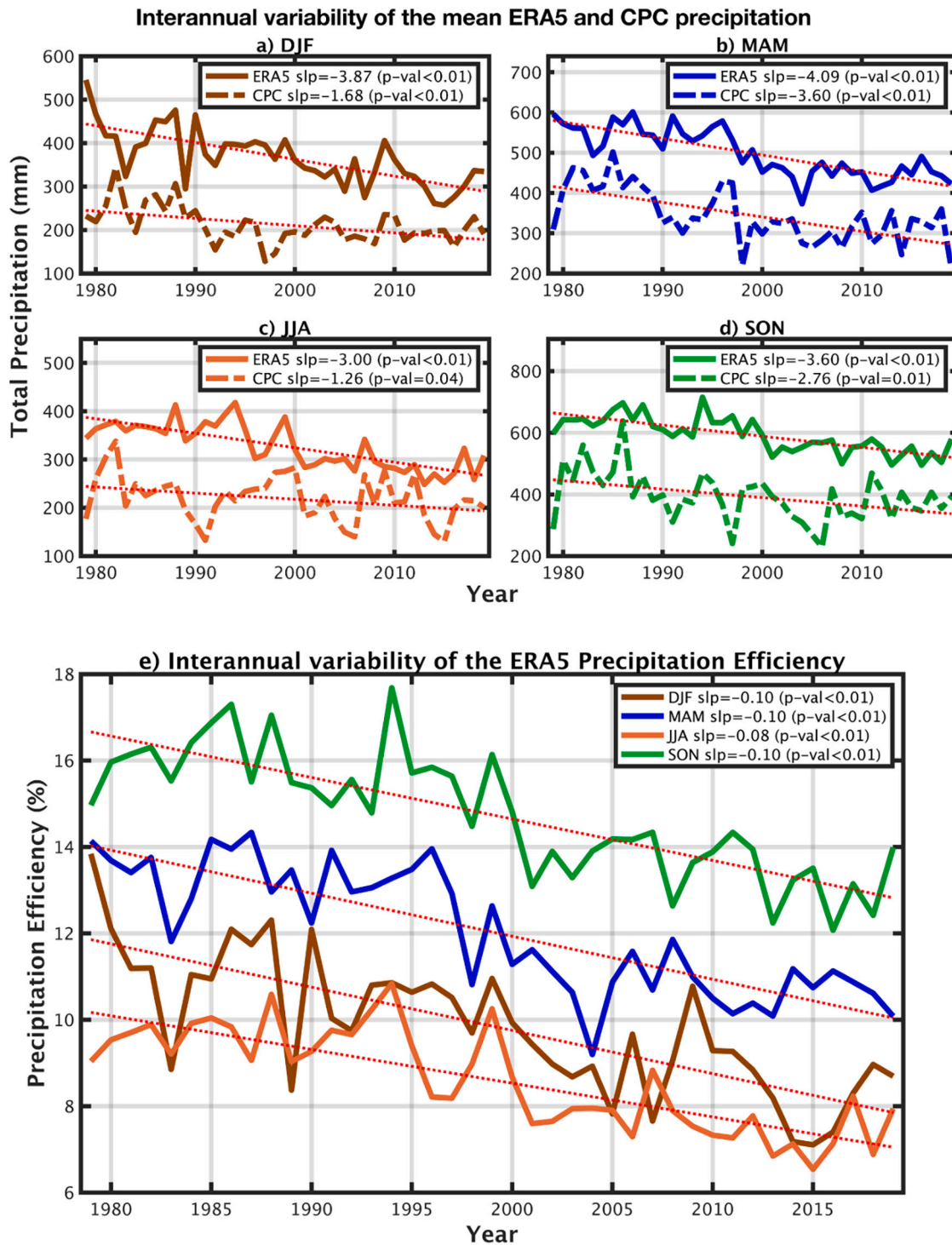


Fig. 9. (a)-(d) Interannual variability and linear trends (mm year^{-1}) of the seasonal mean precipitation from hourly ERA5 and daily CPC data from 1979 to 2019. The ERA5 data is averaged over the study domain, and the CPC data is averaged over the domain 5.25°N to 5.25°S and 12.25°E to 30.25°E . (e) Interannual variability and linear trends ($\% \text{ year}^{-1}$) of the precipitation efficiency, calculated using hourly ERA5 precipitation and ERA5 total column water.

trend over the Congo. Alber et al. (2021) showed that the increase in thunderstorm activity over the Congo might be the result of an increase in the occurrence of cold troughs at 500 hPa, an increase of the temperature gradient between 700 and 950 hPa, and a decrease of the equivalent potential temperature gradient with height. While the increase in the occurrence of cold troughs is potentially the effect of an increased occurrence of Kelvin waves (Raghavendra et al., 2019), the increase of the temperature gradient and the decrease of the equivalent

potential temperature gradient, reducing the vertical stability, may be the result of the observed warming and drying trend of the surface. The enhanced heating and drying during recent years could explain the decrease of clouds in the morning hours and the decrease in the vertical stability of the atmosphere, ultimately enhancing thunderstorm intensity over the region. Consistent with our results, previous studies (e.g., Taylor et al., 2017; Hart et al., 2019) found that MCS frequency is highly correlated with land surface temperatures. Taylor et al. (2017)

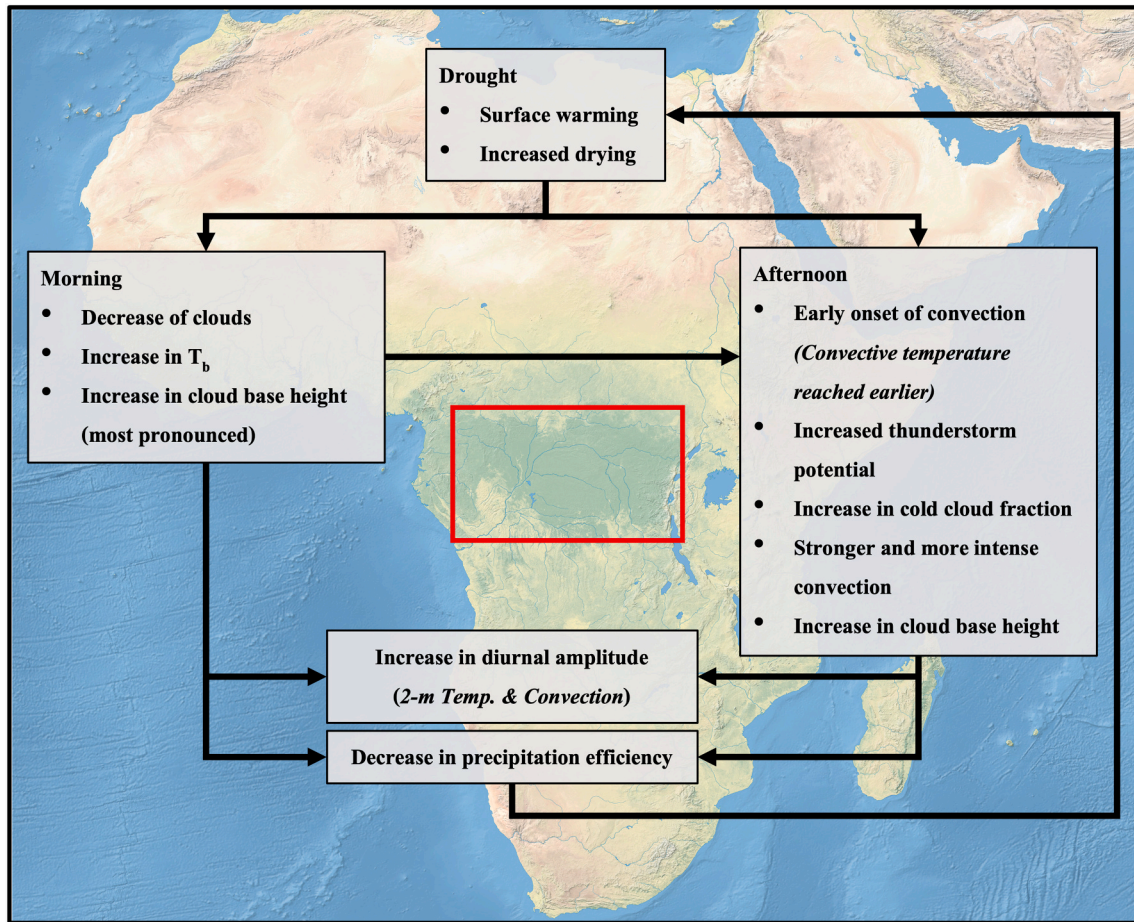


Fig. 10. Proposed potential feedback mechanisms leading to the observed increase in thunderstorm activity, the decrease in precipitation observed at the surface, and the increase in the diurnal amplitude of T2m and convection over the Congo Basin, including a decrease in clouds in the morning and an increase in convection in the afternoon. The study domain is indicated by the red box (Image credits: Background picture made with Natural Earth). (For interpretation of the references to color in this figure legend, the reader is referred to the web version of this article.)

showed intensified Sahelian MCSs as a result of Saharan warming during the months of June–September. They further demonstrate an asymmetric increase in North African temperatures with increased surface warming in the Northern Hemisphere, which might be correlated to the increase in convective activity found over Africa (Hart et al., 2019). Furthermore, other factors like changes in the mid-latitude circulation may have also contributed to the intensifying convection observed over the Congo (Taylor et al., 2018). For example, upper-level troughs forming over Iberia and Northern Africa during the months of November–March have been found to be related to strong MCS events by Ward et al. (2021). The warming and drying of the surface over the Congo could have further led to the observed increase in cloud base height and the subsequent increase in virga, resulting in more precipitation being vaporized before reaching the surface. This might have caused the recorded decrease in precipitation efficiency (-0.08 to -0.10% year $^{-1}$), resulting in the observed decrease of precipitation at the surface, reaching from -3.00 mm year $^{-1}$ to -4.09 mm year $^{-1}$ according to the ERA5 reanalysis dataset, and from -1.26 mm year $^{-1}$ to -3.60 mm year $^{-1}$ according to the CPC dataset. The decrease in precipitation may also be a result of more intense thunderstorms that do not necessarily produce large amounts of precipitation, which has been documented by Hamada et al. (2015) using the Tropical Rainfall Measuring Mission spaceborne radar observations. Therefore, the increased number of thunderstorm cells with increased convective activity observed over the Congo (Raghavendra et al., 2018) possibly also contributes to the decrease in precipitation observed over the region. Additionally, dry air advection from North Africa into the Congo, reduced low-level moisture

transport and enhanced subsidence over the Congo Basin may further reduce relative humidity and decrease precipitation over the region (Jackson et al., 2009; Hua et al., 2016).

Based on our results, we propose some potential feedback mechanisms (Fig. 10) that may help to explain the contrasting trends in deep convection and precipitation over the Congo. The observed drought, enhancing surface warming and drying, may have caused the detected decrease in clouds during the morning, which increases the T_b . These changes may further result in an earlier onset of convection as the convective temperature is reached earlier, and could explain the stronger, more intense convection in the afternoon, ultimately increasing the diurnal amplitude. Additionally, the drying trend possibly caused the increase of the cloud base height and the subsequent increase in virga, decreasing the precipitation efficiency and accelerating the warming and drying at the surface as less precipitation reaches the ground.

In summary, our results showed that the diurnal amplitude of convection over the Congo has increased due to the combined effect of an increase of T_b and a decrease in TCF in the morning, and an increase of deep convection in the afternoon. In the morning, T_b has increased while the cloud cover has decreased, possibly due to the observed warming and drying trend in the study region. The surface warming may also enhance the vertical temperature gradient and decrease the equivalent potential temperature gradient with height, resulting in a decrease in convective inhibition, as suggested by Alber et al. (2021). The decrease in convective inhibition may have caused the increase in thunderstorm activity in the afternoon. While convection has become stronger, precipitation has been shown to decrease. The decrease in precipitation

may be a result of more intense thunderstorm cells producing lower amounts of rainfall, as well as the increased surface warming and drying observed over the region, leading to an increase of the cloud base height and a decrease in precipitation at the surface.

Declaration of Competing Interest

The authors declare that they have no known competing financial interests or personal relationships that could have appeared to influence the work reported in this paper.

Acknowledgments

This work is supported by the National Science Foundation (NSF AGS-1535426 and AGS-1854486). We acknowledge Heather S. Sussman for helping us obtain and process the MODIS dataset. We thank the editor Dr. Cong and two anonymous reviewers for the constructive comments which helped to improve the quality of this paper.

References

- Alber, K., Raghavendra, A., Zhou, L., Jiang, Y., Sussman, H.S., Solimine, S.L., 2021. Analyzing intensifying thunderstorms over the Congo Basin using the Gálvez-Davison index from 1983–2018. *Clim. Dyn.* 56, 949–967.
- Alduchov, O.A., Eskridge, R.E., 1996. Improved magnus form approximation of saturation vapor pressure. *J. Appl. Meteorol.* 35, 601–609.
- Dai, A., 2006. Precipitation characteristics in eighteen coupled climate models. *J. Clim.* 19, 4605–4630.
- Dyer, E.L.E., Jones, D.B.A., Nusbaumer, J., Li, H., Collins, O., Vettoretti, G., Noone, D., 2017. Congo Basin precipitation: assessing seasonality, regional interactions, and sources of moisture. *J. Geophys. Res. Atmos.* 122, 6882–6898.
- Engelbrecht, F., et al., 2015. Projections of rapidly rising surface temperatures over Africa under low mitigation. *Environ. Res. Lett.* 10, 85004.
- Frigo, M., Johnson, S.G., 1998. FFTW: an adaptive software architecture for the FFT. *Proc. IEEE Int. Conf. Acoust. Speech Signal Process.* Seattle, WA 3, 1381–1384.
- Frigo, M., Johnson, S.G., 2005. The design and implementation of FFTW3. *Proc. IEEE* 93, 216–231.
- Gálvez, J.M., Davison, M., 2016. The Gálvez-Davison Index for Tropical Convection. https://www.wpc.ncep.noaa.gov/international/gdi/GDI_Manuscript_V2016_1021.pdf. Accessed 18 May 2021.
- Garreaud, R.D., Wallace, J.M., 1997. The diurnal march of convective cloudiness over the Americas. *Mon. Weather Rev.* 125, 3157–3171.
- Gleixner, S., Demissie, T., Diro, G.T., 2020. Did ERA5 improve temperature and precipitation reanalysis over East Africa? *Atmosphere* 2020 (11), 996.
- Hamada, A., Takayabu, Y.N., Liu, C., Zipser, E.J., 2015. Weak linkage between the heaviest rainfall and tallest storms. *Nat. Commun.* 6, 6213.
- Hart, N.C., Washington, R., Maidment, R.I., 2019. Deep convection over Africa: annual cycle, ENSO, and trends in the hotspots. *J. Clim.* 32, 8791–8811.
- Hersbach, H., et al., 2020. The ERA5 global reanalysis. *Q. J. R. Meteorol. Soc.* 2020, 1–51.
- Hua, W., Zhou, L., Chen, H., Nicholson, S.E., Jiang, Y., Raghavendra, A., 2016. Possible causes of the central equatorial African long-term drought. *Environ. Res. Lett.* 11, 124002.
- Hua, W., Zhou, L., Chen, H., Nicholson, S.E., Jiang, Y., Raghavendra, A., 2018. Understanding the central equatorial African long-term drought using AMIP-type simulations. *Clim. Dyn.* 50, 1115–1128.
- Hua, W., Zhou, L., Nicholson, S.E., Chen, H., Qin, M., 2019. Assessing reanalysis data for understanding rainfall climatology and variability over Central Equatorial Africa. *Clim. Dyn.* 53, 651–669.
- Jackson, B., Nicholson, S.E., Klotter, D., 2009. Mesoscale convective systems over western equatorial Africa and their relationship to large-scale circulation. *Mon. Weather Rev.* 137, 1272–1294.
- James, R., Washington, R., 2013. Changes in African temperature and precipitation associated with degrees of global warming. *Clim. Chang.* 117, 859–872.
- Jiang, Y., Zhou, L., Tucker, C.J., Raghavendra, A., Hua, W., Liu, Y., Joiner, J., 2019. Widespread increase of boreal summer dry season length over the Congo rainforest. *Nat. Clim. Chang.* 9, 617–622.
- Knapp, K.R., 2008. Scientific data stewardship of International Satellite Cloud Climatology Project B1 global geostationary observations. *J. Appl. Remote. Sens.* 2, 023548.
- Knapp, K.R., et al., 2011. Globally gridded satellite observations for climate studies. *Bull. Am. Meteorol. Soc.* 92, 893–907.
- Lau, K.M., Wu, H.T., 2003. Warm rain processes over tropical oceans and climate implications. *Geophys. Res. Lett.* 30, 2290.
- Lutsko, N.J., Cronin, T.W., 2018. Increase in precipitation efficiency with surface warming in radiative-convective equilibrium. *J. Adv. Model. Earth Syst.* 10, 2992–3010.
- Market, P., Allen, S., Scofield, R., Kuligowski, R., Gruber, A., 2003. Precipitation efficiency of warm-season Midwestern mesoscale convective systems. *Wea. Forecasting* 18, 1273–1285.
- National Research Council (NRC), 2004. *Climate Data Records from Environmental Satellites*. National Academies Press, Washington, DC.
- Nicholson, S.E., 2018. The ITCZ and the seasonal cycle over equatorial Africa. *Bull. Am. Meteorol. Soc.* 30, 337–348.
- Pokam, W.M., Djiotang, L.A.T., Mkankam, F.K., 2012. Atmospheric water vapor transport and recycling in Equatorial Central Africa through NCEP/NCAR reanalysis data. *Clim. Dyn.* 38, 1715–1729.
- Raghavendra, A., Zhou, L., Jiang, Y., Hua, W., 2018. Increasing extent and intensity of thunderstorms observed over the Congo Basin from 1982 to 2016. *Atmos. Res.* 213, 17–26.
- Raghavendra, A., Roundy, P.E., Zhou, L., 2019. Trends in tropical wave activity from 1980s–2016. *J. Clim.* 32, 1661–1676.
- Raghavendra, A., Zhou, L., Roundy, P.E., et al., 2020. The MJO's impact on rainfall trends over the Congo rainforest. *Clim. Dyn.* 54, 2683–2695.
- Schiffer, R.A., Rossow, W.B., 1983. The International Satellite Cloud Climatology Project (ISCCP): the first project of the World Climate Research Program. *Bull. Amer. Meteor. Soc.* 64, 779–784.
- Sellers, W.D., 1965. *Physical Climatology*. The University of Chicago Press, 272 pp.
- Soden, B.J., 2000. The diurnal cycle of convection, clouds, and water vapor in the tropical upper troposphere. *Geophys. Res. Lett.* 27, 2173–2176.
- Sui, C.-S., Li, X., Yang, M.-J., 2007. On the definition of precipitation efficiency. *J. Atmos. Sci.* 64, 4506–4513.
- Sun, Q., Miao, C., Duan, Q., Ashouri, H., Sorooshian, S., Hsu, K.-L., 2018. A review of global precipitation data sets: data sources, estimation, and intercomparisons. *Rev. Geophys.* 56, 79–107.
- Taylor, C.M., Belusic, D., Guichard, F., Parker, D.J., Vischel, T., Bock, O., Harris, P.H., Janicot, S., Klein, C., Panthou, G., 2017. Frequency of extreme Sahelian storms tripled since 1982 in satellite observations. *Nature* 544, 475–478.
- Taylor, C.M., Fink, A.H., Klein, C., Parker, D.J., Guichard, F., Harris, P.P., Knapp, K.R., 2018. Earlier seasonal onset of intense mesoscale convective systems in the Congo Basin since 1999. *Geophys. Res. Lett.* 45, 13458–13467.
- Tian, B., Soden, B.J., Wu, X., 2004. Diurnal cycle of convection, clouds and water vapor in the tropical upper troposphere: Satellites versus a general circulation model. *J. Geophys. Res.* 109, D10101.
- Wan, Z., Hook, S., Hulley, G., 2015a. MYD11A2 MODIS/Aqua Land Surface Temperature/Emissivity 8-Day L3 Global 1km SIN Grid V006. NASA EOSDIS Land Processes DAAC.
- Wan, Z., Hook, S., Hulley, G., 2015b. MOD11A2 MODIS/Terra Land Surface Temperature/Emissivity 8-Day L3 Global 1km SIN Grid V006. NASA EOSDIS Land Processes DAAC.
- Ward, Neil, Fink, Andreas, Keane, Richard, Guichard, Françoise, Marsham, John, Parker, Douglas, Taylor, Christopher, 2021. Synoptic timescale linkage between midlatitude winter troughs Sahara temperature patterns and northern Congo rainfall: A building block of regional climate variability. *International Journal of Climatology* 41 (5), 3153–3173.
- Washington, R., James, R., Pearce, H., Pokam, W.M., Moufouma-Okia, W., 2013. Congo Basin rainfall climatology: can we believe the climate models? *Philos. Trans. R. Soc. B* 368, 20120296.
- Yang, G.-Y., Slingo, J., 2001. The diurnal cycle in the tropics. *Mon. Weather Rev.* 129, 784–801.
- Yang, S., Smith, E.A., 2006. Mechanisms for diurnal variability of global tropical rainfall observed from TRMM. *J. Clim.* 19, 5190–5226.
- Zhou, L., et al., 2014. Widespread decline of Congo rainforest greenness in the past decade. *Nature* 509, 86–90.
- Zipser, Edward, Cecil, Daniel, Liu, Chuntao, Nesbitt, Stephen, Yorty, David, 2006. Where are the most intense thunderstorms on Earth? *Bulletin of the American Meteorological Society* 87 (8), 1057–1072.